Thermal decomposed behavior and kinetic study for untreated and flame retardant treated regenerated cellulose fibers using thermogravimetric analysis

F. L. Zhu[1,2] · X. Li[2] · Q. Q. Feng[2]

Abstract

In the present work, pyrolysis kinetic mechanism was studied for regenerated cellulosic fiber (RCF) and composite RCF containing silicon/nitrogen flame retardants. Limited oxygen index and microscale combustion calorimeter tests show that the loading of nitrogen/silicon into the RCF enhanced flame retardancy. The kinetic triplets of the two kinds of samples were determined by applying iso-conversional methods and integral master plots approach. Compared to the untreated RCF, flame retardant (FR) treated RCF shows enhanced activation energy due to the physical barrier layer due to dehydration of silicate and charring effect resulting from organic–inorganic interaction. Exponential nucleation model can be successful in describing experimental results for RCF in higher conversion degree (0.4–0.9). Simultaneously, the degradation process of FR treated RCF in the main pyrolysis stage (0.2–0.7) is consistent with kinetics of nuclei growth and could be described by one-step reaction whose rate presented an Avrami–Erofeev-type model ($n = 2.38$).

Keywords Cellulose fiber · Flame retardant · Kinetic · Thermogravimetric analysis (TGA)

Introduction

Regenerated or artificial cellulosic fibers are manufactured from wood or non-wood biomass pulp [1]. The most widely used regenerated cellulose fibers are fabricated via viscose-rayon procedure though recently many attempts have been made to develop new environmentally friendly solvents to directly dissolve cellulose [2, 3]. Cellulose textile including natural and artificial material has been involved in the daily life as clothing, furniture, and industrial products due to their numerous advantages such as low cost, hydrophilicity, excellent air permeability, and so on [4].

The degradation of cellulose fibers has been studied extensively investigated by many researchers during the last decade. They had made an agreement that the pyrolysis process involves two consecutive reactions: dewatering

and formation of an hydrocellulose at lower temperature (200–280 °C), producing gases and solid residues, and the rapid volatilization of cellulose at higher temperature (280–340 °C) via the formation of Laevoglucosan which will decompose by secondary reaction to low molecular mass products [4–6]. Mathematical modeling of biomass conversion processes and fire clothing protection field can be strongly influenced by which kinetic assumed, so cellulose pyrolytic models have also been intensively surveyed and visited by a great many investigators. However, due to its complex reaction process, the issue on pyrolysis kinetic models of cellulose is still under debate and no actual consensus is arrived. So far, many related kinetic models have been established to understand the decomposition process of cellulosic materials and they differ from the experimental conditions. These models were classified into multi-step kinetic process [7–10], simple first- or nth-order rate expression [11–13] and auto-accelerated reaction process [14, 15]. Among these models, the empirical Broido-Schafizadeh model has been widely accepted to describe cellulose pyrolysis kinetics in terms two parallel (competing) reactions preceded by an initiation step [16]. Recently, a chain scission-driven mechanism has been proposed by Criado et al. [17, 18] to describe the kinetic reaction mechanism

✉ F. L. Zhu
584909509@qq.com

1 College of Clothing, Huizhou University, Huizhou, People's Republic of China

2 College of Textile, Zhongyuan University of Technology, Zhengzhou, People's Republic of China

for cellulose degradation. The developed model involving chain scission and volatilization of fragments made no any previous assumption regarding the reaction kinetic mechanism and using a methodology that does not require the use of complex fitting procedure.

Unfortunately, cellulosic fiber exhibits a low limiting oxygen index, ease of ignition, and high flammability [19]. Moreover, the demands for flame retardant cellulosic textile fabrics used in curtains, upholstery, working clothing, firefighter suits, etc., have a steady growth for the past decades, since numerous injuries and fatalities are caused by fire accidents. Therefore, improvements in flame retardancy of the cellulose fabrics have become one of the important topics. At present, flame retardants, based on halogen, nitrogen, phosphorus, metal oxides, and inorganic compounds in different combinations were widely utilized to impart flame retardancy to cellulosic materials or fabrics [19–24]. Many studies are available in the literature on the thermal degradation behavior of FR treated cellulosic materials. For example, Price et al. [25] proposed a revised model to describe FR cotton material pyrolysis characterized by three stages including stage I (300–400 °C) comprising two competing pathways, stage II (400–800 °C) with aliphatic char converting to an aromatic form, and Stage III (above 800) with char or hydrocarbon further oxidation. Their studies were based on extensive works of a set of commercially flame-retarded cotton (cellulose) fabrics containing condense phosphorus compounds (Amgar TR, Proban CC, Pyrovatex CP) and vapor phase active flame retardants (Amguard CD, Flacavon H14/587) using a range of thermal analysis and FR experimental techniques. Also, the analysis of thermal degradation for FR cellulosic textile imparting by metal oxides (TiO$_2$, ZnO) showed that similar TG/DTG shapes were observed for both samples and decomposition temperature of the treated sample was lower than that of the control sample [26, 27]. As for activation energy, different conclusions were obtained. For instance, Dahiya and Kumar [28] found that activation energy of coated cellulosic fabric with intumescent was lower than that of uncoated sample, and this value further declined on inclusion of metal ions in intumescent formulation. In another case, Gann and Sun concluded that phosphorus FR sample showed increased activation energy of decomposition compared to untreated samples [29]. Aiming at a qualitative understanding in such a variation requires further kinetic analysis of untreated and FR treated cellulosic materials.

To our knowledge, a very limited study on comparisons of pyrolysis kinetic mechanism for non-FR RCFs and FR treated ones based on non-isothermal analysis can be found. This will inhibit the development of new flame retardants for cellulosic materials. Thus, in this work, the flame retardancy and morphology of RCFs was first investigated by different testing approaches including limiting oxygen index (LOI),

TGA, MCC, FTIR, and SEM (EDS). Then, The kinetics of cellulose fiber and its FR hybrid, as well as the activation energies, have been investigated by a combined iso-conversional analysis and master plots procedure at 5, 10, 15, 20, and 25 °C min^{-1} heating rates. A pyrolysis mechanism of FR treated RCF was proposed based on the master plot results.

Materials and methods

Materials

In the present study, non-flame-retarded cellulose fiber—viscose fiber and flame-retarded treated viscose fiber were selected to investigate the thermal kinetics under nitrogen atmosphere. Cellulose fiber (viscose fibers) was purchased from Bailu Chemical Fiber Co. Ltd (Xinxiang China). Silicon FR treated cellulose fibers were supplied by silicon-nitrogen organic

FR treated cellulose fiber (1.5$D \times 38$ mm) was obtained from SOL Flame Retardant Fiber Co. Ltd (Beijing, China). The FR cellulosic fiber was prepared by wet-spinning of regenerated cellulose by adding organosilane hydrolysis dispersion solution into the mucocollagen. The FR chemicals are composed of alkalimetal silicate and amide compounds. The add-on amount of FR chemicals is around 20% mass of cellulose in the coagulation bath consisting of sulfuric acid, zinc sulfate, and aluminum sulfate. These sulfates take their advantages of neutralizing the basicity of sodium silicate. Simultaneously, the acidic environment can promote the thermal degradation of cellulose and accelerate the formation of a carbon layer. The spinned fiber was further fixing crossed by crossing linker containing aluminum ion, calcium ion.

Experimental method

The LOI was measured by using LOI tester (COL, Motis Fire Technology Co Ltd., China). The flammability of cellulosic fiber was evaluated by MCC tests, which were conducted using a FTT0001 microscale combustion calorimeter. The sample, approximately 5 mg, was heated from 125 to 740 °C using a constant heating rate (1 K s^{-1}) in a mixture stream of nitrogen flowing at 80 cm^3 min^{-1} flow rate and oxygen flowing at 20 cm^3 min^{-1}. Non-FR and FR RCFs and their MCC degradation residues in the form of KBr disks were analyzed by Fourier transform infrared (FTIR) spectroscopy using a FTIR spectrometer (Tensor37, Bruker,DE). An average number of 32 scans were taken for each sample with a resolution of 4 cm^{-1}. The used wave range is 4000–400 cm^{-1}. An FE-SEM Quanta 250FEG (FEI) scanning electron microscopes (SEM) was used for observation of the surface morphology of fiber samples. Determination

of the presence of silicon and other elements in the internal structure of the residual char layer was analyzed by using EDAX energy-dispersive spectroscopy (EDS).

Kinetic theory

Thermogravimetric analyzer (TGA) is an important approach to investigate the thermodynamic change process of biopolymer during combustion, gasification, and pyrolysis processes. Due to the complicated chemical pathways and possible intermediates, pyrolysis of cellulose material is a complex process. A full kinetic analysis of the complex system is generally not feasible. However, an overall pyrolysis reaction mechanism is still needed. The primary pyrolysis is represented by the following reaction equation [30]:

cellulose (Solid) → volatile (gases + tar) + Char (solid residue)
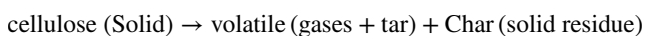
The rate of conversion $d\alpha/dt$ from solid state to the volatile product can be described by the following reaction

$$\frac{\mathrm{d}a}{\mathrm{d}t} = k(T)f(\alpha) \tag{1}$$

where

$$\alpha = \frac{(m_i - m_t)}{(m_i - m_\infty)} \tag{2}$$

In Eq. (2), $f(\alpha)$ is a mechanism model as respects of the conversion degree α. m_i, m_t and m_∞ are the initial sample mass, the sample mass at time t, and the final sample mass remaining at the end of pyrolysis process, respectively. The temperature-dependent reaction rate constant $k(T)$ is expressed by Arrhenius equation as

$$k(T) = A \exp\left(-E_a/RT\right) \tag{3}$$

where A is the pre-exponential factor, E_a is the activation energy of the reaction, and R is the universal gas constant. Equation (4) is obtained by combining Eq. (1) with Eq. (2)

$$\frac{\mathrm{d}\alpha}{\mathrm{d}t} = A \exp\left(-E_a/RT\right)f(\alpha) \tag{4}$$

When the sample is heated to a certain temperature at a constant heating rate $\beta = dT/dt$, Eq. (4) can be rearranged into the following integral form

$$g(\alpha) = \int_0^\alpha \frac{\mathrm{d}\alpha}{f(\alpha)} = \frac{A}{\beta} \int_{T_0}^T \exp\left(-\frac{E_a}{RT}\right) \tag{5}$$

The parameter activation energy (E_a), pre-exponential factor (A), and kinetic model function $f(\alpha)$ are known as kinetic triplets.

Model-free method

Many mathematical models based on the thermogravimetric (TG) data have been applied to describe pyrolytic decomposition mechanism and to determine related kinetic parameters of pyrolysis process, such as activation energy and pre-exponential factor. In general, two types of approaches, iso-conversional (model-free) and model-fitting methods, are employed to evaluate the kinetic parameters during biomass pyrolysis [31]. Model-free methods are iso-conversional methods where the activation energy is a function of the conversion degree. These methods are more reliable than model-fitting methods in evaluating kinetic parameters because they can be utilized without making any assumptions about the reaction function and reaction order. In this work, iso-conversional Kissinger Akahira and Sunose (KAS), Flynn–Wall–Ozawa (FWO), and Starink models which are widely applied for biomass thermal degradation.

Starink examined two the above notable iso-conversional methods and found out that they have the same characteristics of determination of activation energy based on the slope of the logarithmic function containing heat rate β against $1/T$ for each value of α. The Starink equation is very accurate, and hence it is recommendable for use according to ICTAC [32]. These pyrolysis kinetics used to determine activation energies for each conversion ratio are summarized in Table 1.

Integral master plots method

Additionally, the integral form of Eq. (5) can be expressed by a master plot method [38]

$$g(\alpha) = \frac{AE_a}{\beta R}\left[P(u) - P(u_0)\right] \tag{10}$$

where $P(u)$ is temperature integral and $P(u) = \int_\infty^u -(e^{-u}/u^2)\mathrm{d}u$, $u = E_a/RT$ has no exact analytical solution and can be described by

$$P(u) = \frac{\exp(-1.0008u - 0.312)}{u^{1.92}} \tag{11}$$

In general, the pyrolysis rate at ambient temperature T_a is much slower than that the decomposition temperature at the maximum pyrolysis temperature T_{max}. Therefore, the value of $P(u_0)$ can be ignored and Eq. (10) can be integrated as follows:

$$g(\alpha) = \frac{AE_a}{\beta R}P(u) \tag{12}$$

Method	Expression	Plots	References
Kissinger	$\ln\left(\frac{\beta}{T_m^2}\right) = \ln\left(\frac{AR}{E_a}\right) - \frac{E_a}{RT_m}$ (6)	$\ln\left(\frac{\beta}{T_m^2}\right)$ versus $1/T$	[33]
Kissinger Akahira and Sunose (KAS)	$\ln\left(\frac{\beta}{T^2}\right) = \ln\left(\frac{AE_a}{Rg(\alpha)}\right) - \frac{E_a}{RT}$ (7)	$\ln\left(\frac{\beta}{T}\right)$ versus $1/T$	[33, 34]
Flynn–Wall–Ozawa (FWO)	$\log(\beta) = \log\left(\frac{AE_a}{Rg(\alpha)}\right) - 2.315 - 0.4567\frac{E_a}{RT}$ (8)	$\log(\beta)$ versus $1/T$	[35, 36]
Starink	$\ln\left(\frac{\beta}{T^{1.92}}\right) = \text{Const.} - 1.0008\frac{E_a}{RT}$ (9)	$\ln\left(\frac{\beta}{T^{1.92}}\right)$ versus $1/T$	[37]

It is assumed that the pyrolysis reaction occurs in a single-zone process, and the kinetic parameters are constant. Using a reference at point $\alpha = 0.5$, Eq. (11) would be rewritten as

$$g(0.5) = \frac{AE_a}{\beta R}P(0.5) \qquad (13)$$

where $g(0.5)$ is the integral function at $\alpha = 0.5$; $u_{0.5} = E_a/RT_{0.5}$; $T_{0.5}$ is the temperature at $\alpha = 0.5$. By dividing Eq. (12) by Eq. (13), the following master plots formula can be given

$$\frac{g(\alpha)}{g(0.5)} = \frac{P(u)}{P(u_{0.5})} \qquad (14)$$

Plotting $g(\alpha)/g(0.5)$ versus α yields the corresponding theoretical master plots from various, most frequently used

$g(\alpha)$ functions (Table 2). The experimental master plots can be calculated through describing $P(u)/P(u_{0.5})$ against α from experimental data at different heating rates. Equation (12) elaborates that a suitable model can be identified as the best match between the experimental values of $P(u)/P(u_{0.5})$ and theoretical master plots of $g(\alpha)/g(0.5)$.

Results and discussion

Thermal degradation process

The differences in the thermal degradation behavior of a neat viscose fiber and FR treated one were studied by TGA. Figure 1 shows the mass loss and the rate of mass loss profiles of two samples in N_2 under linear heating rate conditions (10 °C min^{-1}). As shown in the figure,

| Reaction mechanism	$f(\alpha)$	$g(\alpha)$
Diffusion models		
One-dimensional diffusion (D1)	0.5α	α^2
Two-dimensional diffusion (D2) (Valensi model)	$[-\ln(1-\alpha)]^{-1}$	$\alpha + (1-\alpha)\ln(1-\alpha)$
Three-dimensional diffusion (D3) (Jander model)	$3/2(1-\alpha)^{2/3}[1-(1-\alpha)^{1/3}]^{-1}$	$[1-(1-\alpha)^{1/3}]^2$
Three-dimensional diffusion (D4) (Ginstling model)	$3/2[(1-\alpha)^{1/3}-1]^{-1}$	$1-2/3\alpha-(1-\alpha)^{2/3}$
Exponential nucleation		
Power law (P2)	$2\alpha^{1/2}$	$\alpha^{1/2}$
Power law (P3)	$3\alpha^{2/3}$	$\alpha^{1/3}$
Power law(P4)	$4\alpha^{3/4}$	$\alpha^{1/4}$
Random nucleation and nuclei growth		
Avrami–Erofeev (A2)	$2(1-\alpha)[-\ln(1-\alpha)]^{1/2}$	$[-\ln(1-\alpha)]^{1/2}$
Avrami–Erofeev (A3)	$3(1-\alpha)[-\ln(1-\alpha)]^{2/3}$	$[-\ln(1-\alpha)]^{1/3}$
Avrami–Erofeev (A4)	$4(1-\alpha)[-\ln(1-\alpha)]^{3/4}$	$[-\ln(1-\alpha)]^{1/4}$
Order of reaction		
First-order (F1)	$1-\alpha$	$-\ln(1-\alpha)$
Second-order (F2)	$(1-\alpha)^2$	$(1-\alpha)^{-1}-1$
Third-order (F3)	$(1-\alpha)^3$	$[(1-\alpha)^{-2}-1]/2$
Geometrical contraction models		
Contracting cylinder (R2)	$2(1-\alpha)^{1/2}$	$1-(1-\alpha)^{1/2}$
Contracting sphere (R3)	$2(1-\alpha)^{2/3}$	$1-(1-\alpha)^{1/3}$
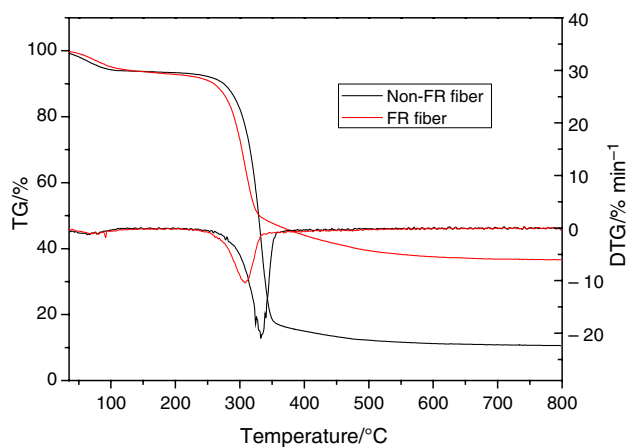
Fig. 1 TG and DTG graph of non-FR and FR treated RCF at 10 °C min⁻¹ heating rate

the pyrolysis of untreated RCF takes place in three steps: initial, main and char decomposition. The first step occurring below 260 °C was due to the moisture desorption and highly volatile matters in the samples. The main pyrolysis was observed in the temperature range of 260–380 °C. At this stage, a drastic 72% mass loss occurs with 120 °C temperature increment, which may be was associated with volatilization resulting in the formation of levoglucosan, and levoglucosan decomposed further to low molecular mass products. The third stage is the char pyrolysis occurred at temperature above 380 °C. Most of the mass residue (15.8%) is observed up to 380 °C when compared to the maximum mass residue (10.6%) which is acquired at an 800 °C. This illustrates that no more mass conversion reactions take place at temperatures higher than 380 °C. In this process, dewatering and charring reactions compete with the production of levoglucosan, but the charring reactions is in a dominant position.

The TG/DTG curves for the FR samples take similar shapes as those of untreated RCF and three regions could be also observed. At about 85 °C (moisture desorption at this stage), the remaining mass of FR treated fibers is slightly lower than that of untreated samples, which indicates a little better moisture absorption performance of untreated RCF. It can be noticed that the onset of degradation of the FR composite fiber was advanced to a lower temperature. Also from Table 3, the maximum decomposition temperature (308 °C) of FR treated sample is about 24.5 °C lower than that (332.5 °C) of the untreated RCF. This can be explained by two facts. The first fact is that a small amount of sulfates remain in the RCF produce an acidic environment and accelerate the thermal degradation of cellulose fiber [39]. The other is that the first decomposition of amide compounds releasing gas also causes a decrease in the pyrolysis temperature. On the other hand, inorganic silica incorporated into cellulose fiber could significantly delay the initial decomposition temperature because silica coating acted as physical barrier that hindered thermal energy transfer between the gas and solid phase [22]. But the values of derivative for FR samples are lower than those of untreated cellulose hybrids which elucidating clearly that the addition of sodium silicate can slow down the rate of degradation of cellulose fibers and further prevent the polymeric structure from degrading. Overall, the entire thermal decomposition process of non-FR treated cellulosic materials is later than that of FR treated cellulosic ones. This indicates that the thermal stability of the cellulose fibers with silicon/nitrogen components has not been improved as compared to the untreated fibers in terms of thermal degradation analysis experiments. By contrast, other flame retardants such as zinc ion can effectively promote thermal stability of cellulose materials when appropriate contents were contained [27].

The initial decomposition temperature T_{ini} at the mass loss of 10% and maximum mass loss temperature T_m at five

Table 3 Characteristic temperature data for degradation and Kissinger kinetic parameters untreated and FR treated RCF

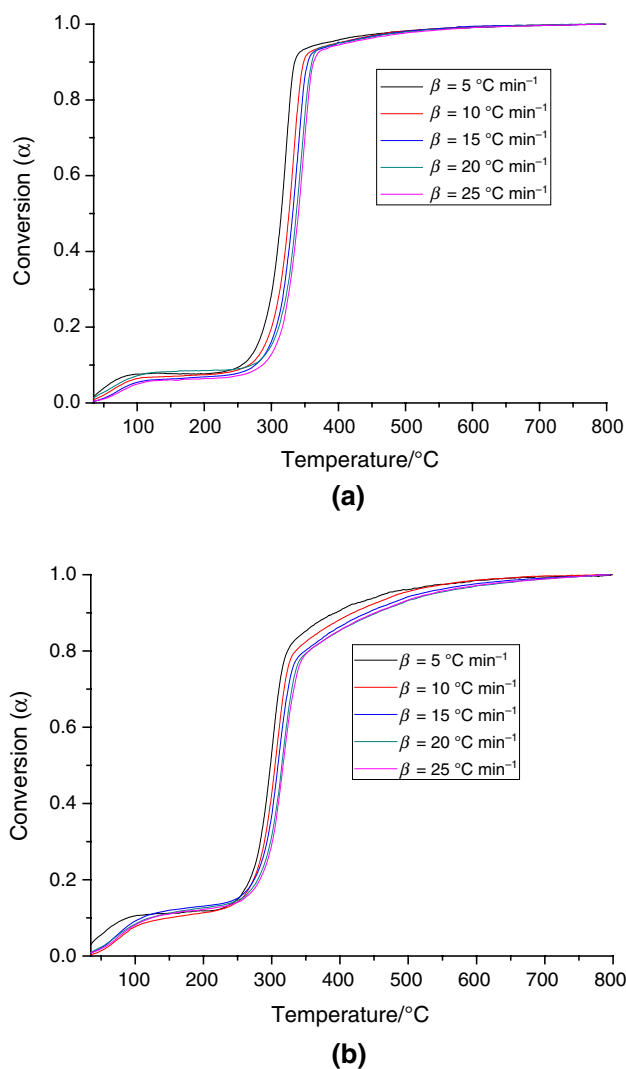| Sample	Heating rate/°C min⁻¹	T_{ini} (mass loss at 10%)/°C	Tm (peak DTG)/°C	Char remains at 500 °C (%)	Kissinger method		
					Activation energy/kJ mol⁻¹	Pre-exponential factor/s⁻¹	Adj. R^2 coefficient
Untreated RCF	5	264.5	322.0	12.49	162.17	$5.04×10^{10}$	0.9741
	10	275.0	332.5	12.24			
	15	283.5	339.0	12.49			
	20	281.0	348.0	10.64			
	25	292.5	349.0	11.66			
FR treated RCF	5	254.5	299.5	39.01	278.59	$1.33×10^{22}$	0.9562
	10	259.5	308.0	39.40			
	15	252.5	309.0	38.75			
	20	254.0	313.5	37.49			
	25	260.5	315.0	37.57			

Fig. 2 Evolution of conversion α with temperature T for various heating rates (**a** untreated RCF; **b** FR treated RCF)

heating rates are summarized in Table 3. As the heating rate increased, Table 3 shows that there were lateral shifts to higher temperature for T_m. These shifts are also illustrated in Fig. 2. An increase in the heating rate of the sample caused displacement of pyrolysis conversion α to higher temperature. As the temperature continues to increase from 380 to 800 °C, a significantly large amount of solid residues is produced from cellulose-nitride/silicon fibers. On the other hand, the FR treated fiber has a 36.61% by mass of char residue at the temperature of 800 °C, indicating a significant increase in char formation at 800 °C compared to the referred neat cellulose sample (10.58%). In principle, the charring residues can insulate the surface acting as a barrier to the release of heat and volatile compounds to prevent further decomposition, so the amount of char residue formed in the thermal degradation provides quantitative information

on the flame retardant performance of a biopolymer [40]. An enhanced char formation over this temperature region corresponds to better flame retardant capacity. The nitrogen and silicon containing fire retardant induces the dehydration of the FR fibers and generates the compact and stable char. Obviously, the TG result shows that cellulose fiber containing nitrogen and silicon exhibited excellent efficiency in flame retardancy compared to the fiber without flame retardants.

Flame retardant and combustion properties of cellulose fibers

The LOI method was applied to evaluate the ignition and flame retardant behavior of a sample. The approach is also a quantitative and qualitative technique with wide spread use in both academic research and industry. The LOI values of the non-FR and FR RCFs are 19.5 and 28.5, respectively. In general, fiber materials can be regarded as be flame retardant when LOI values is higher than 26. So, the FR chemicals including nitrogen and silicon impart flame retardancy for RCF. As we known, MCC is evaluated as a screening test for efficacy of flame retardant in polymers from just a few milligrams of specimen. The related flammability parameters provided by a single MCC experiment include heat release rate (HRR), heat release capacity (HRC), total heat release (THR), peak heat release rate (pHRR), and temperature at pHRR (T_{pHRR}). Table 4 shows

Table 4 Combustion data recorder in MCC experiments

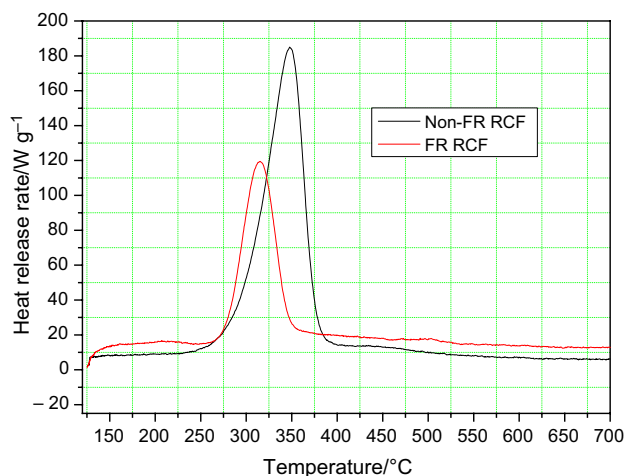| Samples	pHRR/W g^{-1}	HRC/J g^{-1} K^{-1}	T_{pHR}/°C	THR/kJ g^{-1}
Non-FR RCF	177.6	180	341.4	10.5
FR RCF	105.7	108	313.0	5.9

Fig. 3 Heat release curves of FR and non-FR treated RCF

pHRR, HRC, THR ,and T_{pHRR} of the FR and non-FR cellulosic fibers conducted by MCC tests. Figure 3 shows the heat release rate (HRR) curves of the fibers as a function of the heating temperature. It is observed from the figure that the thermal decomposition of the non-FR RCF started at approximately 295 °C. The decomposition, as indicated by ascending HRR, augmented as the temperature increased. It reaches to maximum at 341.4 °C with HRR at 177.6 W g^{-1} (pHRR). Compared to the non-FR fiber, significant changes in the MCC parameters when the fiber were treated by FR silicon elements. The pHRR and THR of the FR sample decrease to 105.7 W g^{-1} (40.5% reduction) and 5.9 kJ g^{-1} (43.8% reduction). This implies peak temperature T_{pHRR} shifted from 341.4 to 313.0 °C. Moreover, the initial decomposed temperature is ahead to about 247 °C. The pyrolysis temperature values also support the results of the TG experiments. It can be said that the presence of sodium silicate reduces the pyrolysis temperature and effectively improves the flame retardancy of RCFs. Like TG analysis, this advanced phenomenon of pyrolyzed temperature is attributed to the first decomposition of sodium silicates. In addition, a glassy layer, which forms due to dehydration of sodium silicate on the surface of the combustion fiber, will prevent oxygen from being diffused into the flammable matrices [41].

FTIR spectroscopy

FTIR spectroscopy has been used as a simple technique for acquiring rapid information about the change of surface composition of fiber after thermal degradation and FR treatment. For the neat RCF, the spectra can be separated into two regions: the O–H and C–H stretching vibrations in the 4000–2700 cm^{-1}, and the "fingerprint" region, which is related to different stretching vibration of different groups in the 1800–500 cm^{-1} region [42]. But the spectra of 700 °C residue show that decomposition of glycopyranose ring is elucidated by the disappearance of bands at 1600 cm^{-1}(C=C stretching), 1400 cm^{-1} (CH$_2$ symmetric bending), 1370 cm^{-1} (CH bending) and 820 cm^{-1} (out-of-plane bending of C–H vibration). The feature at 2300 cm^{-1} is related to O–H stretching [43]. As was observed from silicate FR cellulose fiber, the peak caused by O–H stretching vibration at 3400 cm^{-1} is considerably reduced. The differences between the FTIR spectra of FR RCF and non-FR RCF reveal a decrease in the hydroxyl group content due to reaction between –OH and silicate [44]. Compared to non-FR RCF, FR RCF possesses stronger band intensities around 1000–600 cm^{-1}. The presence of the silicate results in the Si–O–Si bending mode adsorption at 810 cm^{-1} which is overlapped with out-of-plane C–H bending vibration [45] (Fig. 4).
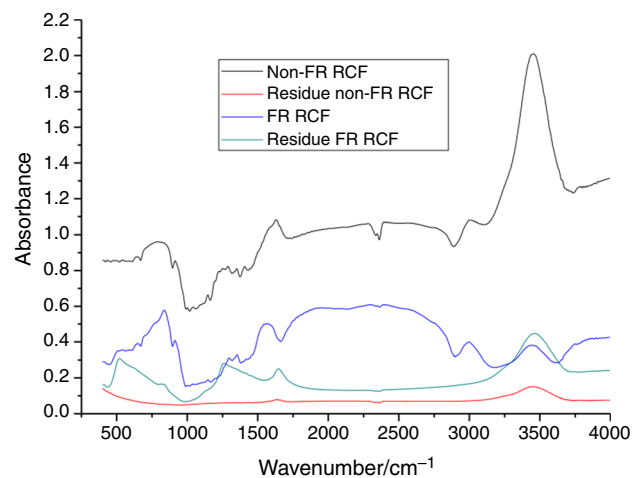

Fig. 4 FTIR spectra of cellulosic fibers: **a** non-FR RCF, **b** residue non-FR RCF, **c** FR RCF, **d** residue FR RCF

SEM images of RCFs and their char residues

SEM analysis was used to characterize any changes in the surface morphology of fiber. Representative SEM micrographs, taken at the magnification of 5000 of non-FR and FR RCFs, are shown in Fig. 5. The SEM images of their residues are also illustrated in Fig. 5c and d. As can be seen from the SEM images, there are parallel grooves and cracks that run alongside the fiber axis for both two kinds of cellulosic fibers. This is because the fiber volume shrinking reduces and folds form on the surface of fiber due to the internal moisture removal of fine flow after the film layer formed by viscose fine flow. By comparison, the surface morphology of flame retardant cotton fiber is coarser, which is due to the crosslinking reaction between crosslinker and the fiber as described in the Materials section. An examination of the microstructures of the residue of treated and untreated fiber shows that the surface of non-FR sample is relatively flat smooth compared with the figure of FR sample. Residual char of FR sample has loose, typical residue microstructure, and the reason may be amide compounds as gas source decomposes and releases gas which finally formed a loose structure [46]. EDS measurement results (Fig. 5e and f) indicate that the char residue of FR RCF consists of a large amount of Si element (mass 5.06%), which is only mass 0.23% for non-FR RCF. Silicon elements in non-FR RCF may come from silicon oil in the softening finishing process. In addition, the sodium (Na), the aluminum (Al), and the calcium (Ca) were detected in the residue of FR RCF.
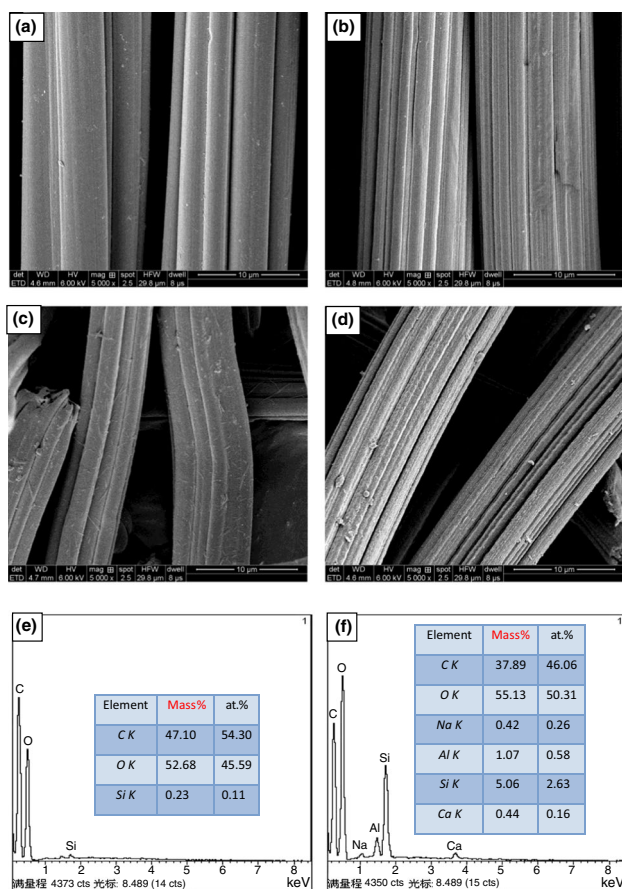
Fig. 5 SEM micrographs of RCFs: **a** non-FR RCF; **b** FR RCF; **c** residue of non-FR RCF; **d** residue of FR RCF. EDS spectrum of char residual **e** non-FR RFC; **f** FR RCF

Kinetics

Kinetic parameters estimation

The results from TGA of the untreated and FR treated RCF at five heating rates (5, 10, 15, 20, and 25 °C min^{-1}) can be used to determine the kinetic parameters like activation energy and pre-exponential factor by using model-free methods. The drying behavior of fiber will be investigated in the further work by thermogravimetric analysis under non-isothermal condition. Moreover, the termination of solid-state reactions is unstable. Therefore, the conversion range of 0.2–0.9 with an increment of 0.1 under each heating rate was used for kinetic analysis in this study. Little correlation was observed for valuations of conversion below 0.2 and above 0.8.

According to Eq. (6), the Kissinger method was first employed to calculate kinetic parameters by plotting ln(β/T_m) versus 1/T, and the plots are shown in Fig. 6. The peak temperature (T_m) obtained from the DTG data and the kinetic parameters for sample pyrolysis are tabulated in Table 3.

T_m increased with the increase in heating rate. The slope of the plots yielded activation energies of 162.17 kJ mol^{-1} for untreated cellulose sample and 278.59 kJ mol^{-1} for FR treated one. This evident discrepancy can be explained by that the Kissinger method employs only the information related to the maximum rate of reaction to obtain unique values for activation energy and pre-exponential factor.

Linear fit plots of various Y-axis functions against 1/T are made to determine the activation energy (E_a) values using KAS, FWO, and Starink methods, and graphs are presented in Fig. 7. Thermal kinetics of the first region which was due to moisture, and highly volatile matters are not calculated as the process is related to drying kinetics.

The calculated energies for different conversion values and the corresponding correlation factors using KAS, FWO, and Starink models are listed in Table 5. The adjusted correlation coefficients (R^2) by the three methods for non-FR fiber are close to 1 for these mentioned conversions (0.2–0.9). It is found from Table 5 that these three iso-conversional methods yield similar values of activation energy for the untreated and FR treated samples as all of them are integral methods that are derived from the same general expression. The average values of activation energy E_a of non-FR and FR fabrics are 171.89 and 195.92 kJ mol^{-1} by KAS method, 173.03 and 195.81 kJ mol^{-1} by FWO method, 172.23 and 196.25 kJ mol^{-1} by Starink method, respectively. The maximum deviations of average E_a values for the two kinds of fabrics among these three methods are less than 0.7% and 0.3%. These E_a values can be acceptable within 2% of the lower value. The average activation energies of FR treated RCF are higher than that of non-FR treated calculated data no matter what iso-conversional method is used to determine the E_a value. It is known that activation energy, which is used to describe the energy barrier overcome for a chemical reaction, is regarded as a minimum energy to make a thermal degradation reaction happen. Higher the activation energy, slower the pyrolysis reaction. The finding of the higher activation energy for the considering conversion range of the FR treated RCF indicates that the energy barrier of the decomposition of the treated FR RCF is enhanced due to chemical disposal. The inclusion of nitrogen and silicon compounds into fibers would improve the thermal stability for cellulose fibers in terms of the increased apparent activation energy.

There are similar disciplines on activation energies of other organic chemicals treated cellulosic or lignocellulosic materials [20, 47]. However, the opposite conclusion that lower activation energies were presented as a result of inorganic chemical FR treatment in cellulosic or lignocellulosic materials could be found in the literatures [28, 39, 48, 49]. Though appropriate inorganic ingredients could improve the flame resistant performance, the thermal stability of inorganic FR cellulose is depressed with the representation of the decrease in the activation energy [50]. On the contrary,
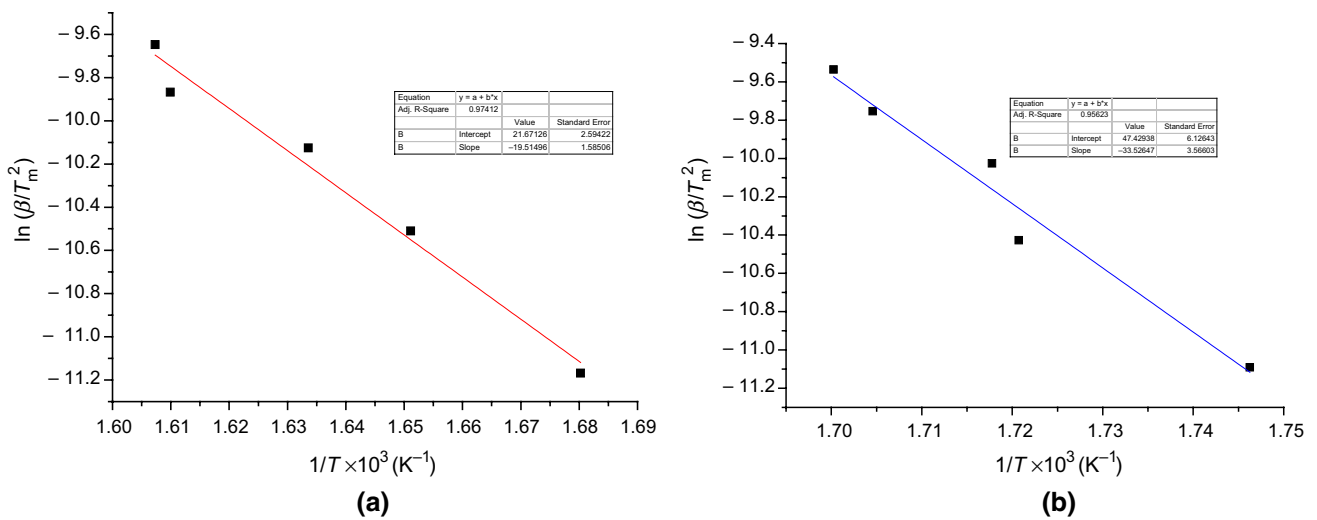
Fig. 6 Linear plots by the Kissinger method of untreated (**a**) and FR treated (**b**) RCF

the increased activation energy of FR samples with organic nitrogen–silicon elements is related to the charring effect generated by organic interaction reaction.

The variation in activation energy with progress in conversion is shown in Fig. 8. It is observed the calculated E_a values varied with conversion points and were shown to be significantly decreased as conversion increased further for FR treated cellulose samples. The decrease in activation energy, especially at the later stage (conversion 0.7–0.9), indicates the presence of exothermic reactions due to more char formation (exothermic process) with dewatering and decarboxylation reaction catalyzed by flame retardants. Simultaneously, high dependence of activation energy on conversion also means that pyrolysis of FR treated RCF is
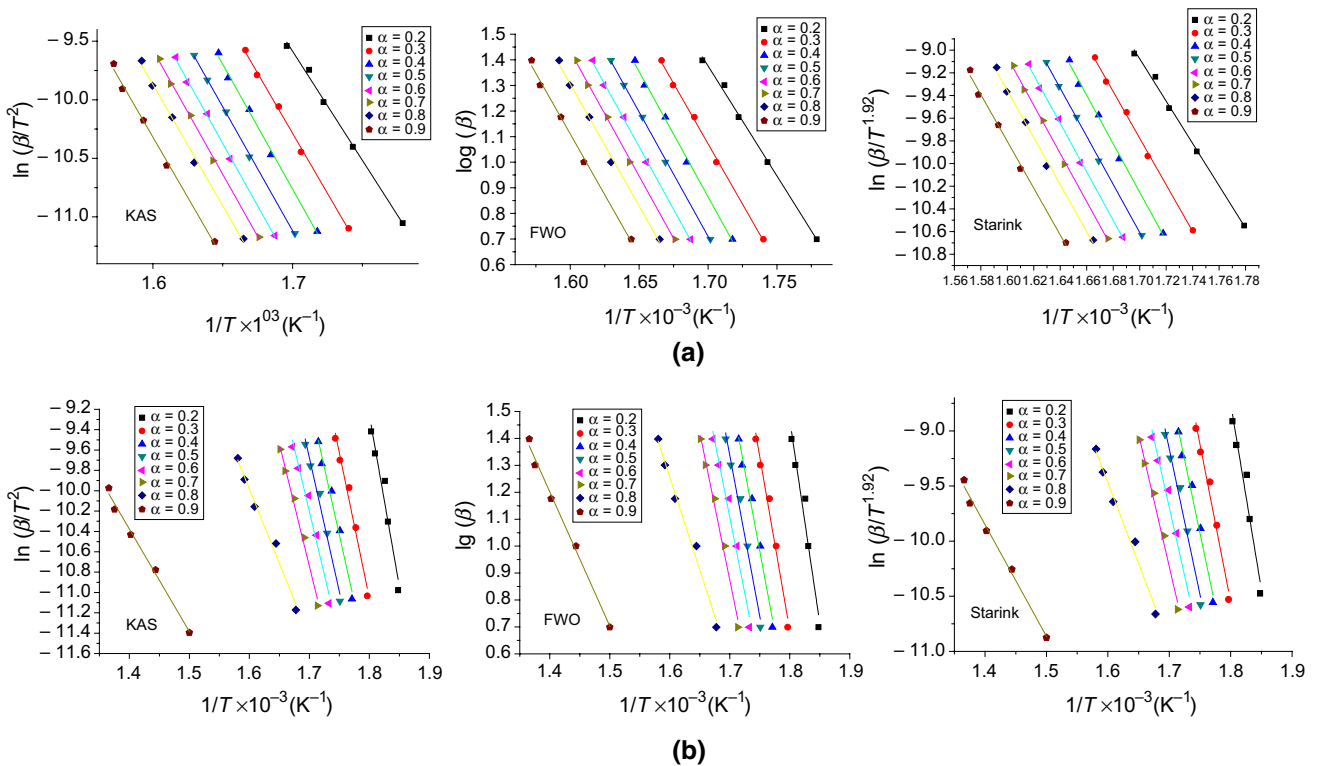

Fig. 7 Linear plots for determination of activation energy at different conversion by Friedman, KAS, FWO, and Starink methods for untreated (**a**) and FR treated (**b**) RCF

Table 5 E_a values calculated from each iso-conversional methods

| Conversion (α) | KAS model | | | | FWO model | | | | Starink model | | | |
| | Untreated | | FR treated | | Untreated | | FR treated | | Untreated | | FR treated | |
	E_a kJ mol^{-1}	R^2	E_a kJ mol^{-1}	R^2	E_a kJ mol^{-1}	R^2	E_a kJ mol^{-1}	R^2	E_a kJ mol^{-1}	R^2	E_a kJ mol^{-1}	R^2
0.2	154.84	0.9950	279.74	0.9377	156.41	0.9956	274.81	0.9414	155.18	0.9950	280.02	0.9378
0.3	170.47	0.9973	237.32	0.9745	171.47	0.9976	234.72	0.9765	170.81	0.9973	237.62	0.9746
0.4	177.08	0.9958	219.99	0.9788	177.87	0.9962	218.37	0.9806	177.42	0.9958	220.28	0.9789
0.5	175.79	0.9991	218.98	0.9780	176.74	0.9992	217.53	0.9799	176.13	0.9991	219.30	0.9781
0.6	177.22	0.9983	206.44	0.9698	178.17	0.9984	205.70	0.9725	177.56	0.9983	206.77	0.9699
0.7	176.30	0.9976	199.56	0.9853	177.37	0.9978	199.26	0.9867	176.65	0.9976	199.89	0.9853
0.8	172.15	0.9951	121.54	0.9815	173.49	0.9956	125.34	0.9843	172.50	0.9951	121.91	0.9816
0.9	171.24	0.9947	83.78	0.9901	172.76	0.9952	90.76	0.9826	171.60	0.9947	84.22	0.9902
Average	171.89	–	195.92	–	173.03	–	195.81	–	172.23	–	196.25	–
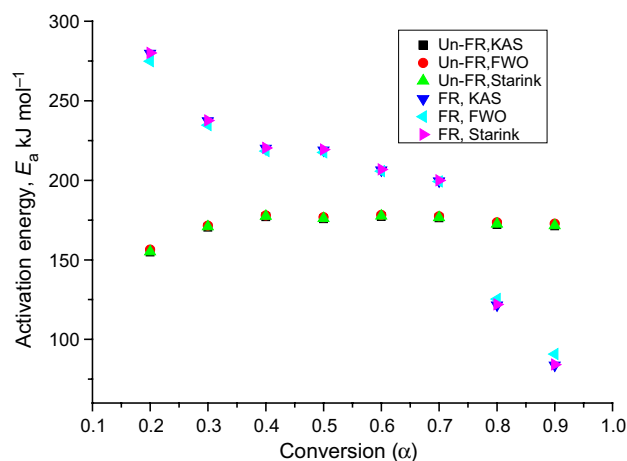
Fig. 8 Activation energies of RCF versus conversion degree by KAS, FWO and Starink methods

a more complex process involvement of parallel, competitive reactions, and FR components' interactions. By contrast, activation energy values only slightly ascended at the early stage ($\alpha < 0.4$) and were fairly constant in the remaining conversion process. As can also be seen from Table 4 and Fig. 5, the obtained activation energy values from KAS, FWO, and Starink methods were close to the previously reported values for neat cellulose materials [51].

Kinetic mechanism

The average activation energy values obtained from Starink methods were utilized in the integral master plots methods to find the pyrolysis kinetic models which can describe the experimental data better. The master plots are independent of the heating rates, and these experimental points take similar trends [18]. Hence, the master plots of $g(\alpha)/g(0.5)$ against α corresponding to the theoretical master plots for various kinetics models (Table 2) at 10 °C min^{-1} are only constructed at the heating rate of 10 °C min^{-1} and are illustrated in Fig. 9. ICTAC Kinetic committee recommended that the Starink isoconversion method was suitable to calculate the activation energy accurately. Thus, the E_a values obtained from Starink method would be used in the above master plots method to find the reaction model.

The experimental master curves of untreated RCF are well matched with the theoretical exponential nucleation models (P2, P3, and P4 models). The results obtained from the comparisons between experimental master plots, and these theoretical curves indicate that P4 model may be most suitable equation to characterize the pyrolysis of untreated samples in the range of conversion 0.4–0.9 (Fig. 9a). But it is not completely fit with large dispersity appeared at lower conversion (0.2–0.4). As can be also seen in Fig. 9b, the experimental curve of FR treated RCF is not well coincided
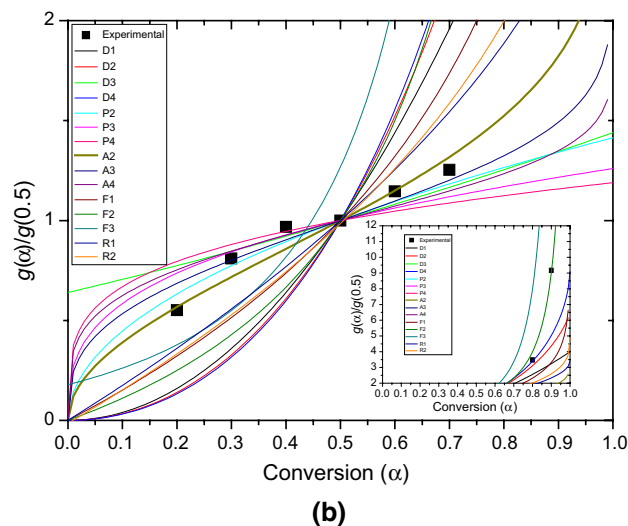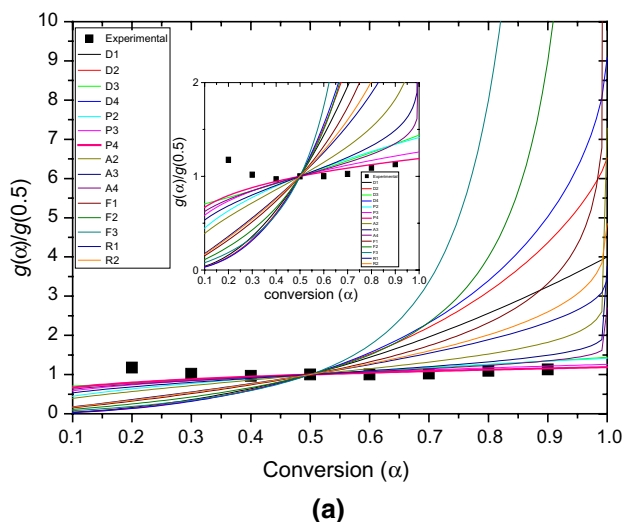
(a)

(b)

Fig. 9 Comparison between experimental scatter dots and theoretical master plots constructed from the kinetic functions with linear heating rate of 10 °C min^{-1}

with any the theoretical master plot $g(\alpha)/g(0.5)$, whereas it appears that the experimental plot at 20–70% conversion showed a sigmoid profile, which is similar with an auto-accelerated reaction process. Thus, the random nucleation growth model (Avrami–Erofeev type) may be suitable to simulate the pyrolysis of FR treated cellulose at the main pyrolysis stage. According to Fig. 9b, a jump phenomenon (the experimental plots serious deviation from the A_n theoretical curves) is found when α is greater than 0.7 and the FR sample decomposition mechanism may change, which implies that multistage mechanisms occur until the final conversion. Accordingly, the pyrolysis kinetic mechanism of the FR treated RCF should be given in the conversion range of 0.2–0.7 instead of the whole thermal degradation process. Then, A_n function (Table 2) is used to calculate the kinetic
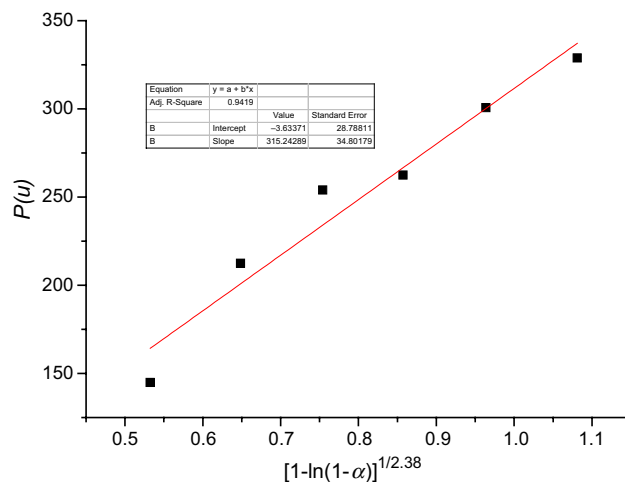

Fig. 10 Linear plot of $[-\ln(1-\alpha)]^{1/n}$ against $P(u)$

exponent (n) and pre-exponential factor (A), and the following formula can be given based on the Avarmi–Erofeev-type kinetic equation in the form of $[-\ln(1-\alpha)]^{1/n}$.

$$g(\alpha) = \frac{AE_a}{\beta R}P(u) = [-\ln(1-\alpha)]^{1/n}$$

After obtaining the primary description on the kinetic mechanism, a sigmoidal curve fitting to the experimental data according to the definition function by the first Opt code with the Levenberg–Marquardt method was found the exact n value. The pre-exponential factor A value can be calculated from the slope of linear fitting plot of $[-\ln(1-\alpha)]^{1/n}$ against $P(u)$ (Fig. 10). As a result, the experimental master plots locate the theoretical master plots $A_{2.38}$, the pre-exponential factor $A = 8.62 \times 10^6$ at 10 °C min^{-1}. Then, the nucleation growth function $g(\alpha) = [-\ln(1-\alpha)]^{1/2.38}$ could be acquired for describing pyrolysis of FR RCF in the conversion range of 0.2–0.7.

Conclusions

Flame retardant properties of FR and non-FR RCF were evaluated by LOI, TGA, MCC, and FTIR measurements. These FR analyses show that the RCF with silicon/nitrogen components exhibits a different thermal behavior from that the non-FR cellulosic fiber. It is found that, as compared with the non-FR RCF, the onset degradation temperature T_{ini} and maximum decomposition temperature T_{max} of the FR composite fiber are advanced to a lower temperature. The phenomenon can also be observed in the MCC measurements. Kinetics of the non-isothermal degradation of untreated and FR treated RCF is also analyzed using iso-conversional kinetic methods at different

heating rates. The values of the samples have the same sequence obtained by KAS, FWO, and Starink techniques. The kinetic results show that the activation energy for degradation of FR treated RCF is much higher than that of neat RCF, suggesting that FR treatment on a RCF has a great effect on the decomposition capacity (Characterized by activation energy) of RCF. It is likely that the apparent mechanism of overall reaction cannot be expressed in terms of one simple reaction model. Nevertheless, in a certain conversion range (0.2–0.7), pyrolysis mechanism of FR treated RCF can be described by nucleation growth model of $g(\alpha) = [1 - \ln(\alpha)]^{1/2.38}$.

References

1. Uddin AJ, Yamamoto A, Gotoh Y, Nagura M, Iwata M. Preparation and physical properties of regenerated cellulose fibres from sugarcane bagasse. Text Res J. 2010;80(17):1846–58.
2. Perepelkin KE. Lyocell fibres based on direct dissolution of cellulose in N-methymorpholine N-oxide: development and prospects. Fibre Chem. 2007;39:163–72.
3. Calvin W. Regenerated cellulose fibres. Manchester: Textile Institute; 2001. p. 5.
4. Wang S, Lu A, Zhang L. Recent advances in regenerated cellulose materials. Prog Polym Sci. 2016;53:169–206.
5. Zhu P, Sui SY, Wang B, Sun K, Sun G. A study of pyrolysis and pyrolysis products of flame-retardant cotton fabrics by DSC, TGA, and PY-GC-MS. J Anal Appl Pyrolysis. 2004;71:645–55.
6. Kandola BK, Horrocks AR, Price D, Coleman GV. Flame-retardant treatments of cellulose and their influence on the mechanism of cellulose pyrolysis. J Macromol Sci C Polym Rev. 1996;36(4):721–94.
7. Abdelouahed L, Leveneur S, Vernieres-Hassimi L, Balland L, Taouk B. Comparative investigation for the determination of kinetic parameters for biomass pyrolysis by thermogravimetric analysis. J Thermal Anal Calorim. 2017;129:1201–13.
8. Bradbury AGW, Sakai Y, Shafizadeh F. Kinetic model for pyrolysis of cellulose. J Appl Polym Sci. 1979;23:3271–80.
9. Alves SS, Figueiredo JL. Pyrolysis kinetics of lignocellulosic materials by multi-stage isothermal thermogravimetry. J Anal Appl Pyrolysis. 1988;13(1–2):123–34.
10. Conesa JA, Caballero JA, Marcilla A, Font R. Analysis of different kinetic model, in the dynamic pyrolysis of cellulose. Thermochim Acta. 1995;254:175–92.
11. Suriapparao DV, Ojha DK, Ray T, Vinu R. Kinetic analysis of co-pyrolysis of cellulose and polypropylene. J Thermal Anal Calorim. 2014;117:1441–51.
12. Baroni EG, Tannous K, Rueda-Ordonez YJ, Tinoco-Navarro LK. The applicability of isoconversional models in estimating the kinetic parameters of biomass pyrolysis. J Thermal Anal Calorim. 2016;123:909–17.
13. Alves SS, Figueiredo JL. Kinetics of cellulose pyrolysis modelled by three consecutive first-order reactions. J Anal Appl Pyrolysis. 1989;17(1):37–46.
14. Burnham AK, Zhou XW, Broadbelt LJ. Critical review of the global chemical kinetics of cellulose thermal decomposition. Energy Fuels. 2015;29(5):2906–18.
15. Capart R, Khezami L, Burnham AK. Assessment of various kinetic models for the pyrolysis of a microgranular cellulose. Thermochim Acta. 2004;417:79–89.
16. Lin YC, Cho JM, Tompsett GA, Westmoreland PR, Huber GW. Kinetics and mechanism of cellulose pyrolysis. J Phys Chem C. 2009;113:20097–107.
17. Sanchez-Jimenez PE, Perez-Maqueda LA, Perejon A, Pascual-Cosp J, Benitez-Guerrero M, Criado JM. An improved model for the kinetic description of the thermal degradation of cellulose. Cellulose. 2011;18:1487–98.
18. Sanchez-Jimenez PE, Perez-Maqueda LA, Perejon A, Criado JM. Generalized master plots as a straightforward approach for determining the kinetic model: the case of cellulose pyrolysis. Thermochim Acta. 2013;552:54–9.
19. Abou-Okei A, El-Sawy SM, Abdel-Mohdy FA. Flame retardant cotton fabrics treated with organophosphorous polymer. Carbohyd Polym. 2013;92(2):2293–8.
20. Moafi HF, Shojaie AF, Zanjanchi MA. Flame-retardancy and photocatalytic properties of cellulosic fabric coated by nano-sized titanium dioxide. J Therm Anal Calorim. 2011;104:717–24.
21. Horrocks AR, Kandola BK, Davies PJ, Zhang S, Padbury SA. Developments in flame retardant textiles—a review. Polym Degrad Stabil. 2005;88(1):3–12.
22. Hribernik S, Smole MS, Kleinschek KS, Bele M, Jamnik J, Gaberscek M. Flame retardant activity of SiO_2-coated regenerated cellulose fibres. Polym Degrad Stabil. 2007;92(11):1957–65.
23. Yang ZY, Wang XY, Lei DP, et al. A durable flame retardant for cellulosic fabrics. Polym Degrad Stabil. 2012;97(11):2467–72.
24. Kivotidi S, Tsioptsias C, Pavlidou E, Panayiotou C. Flame-retarded hydrophobic cellulose through impregnation with aqueous solutions and supercritical CO_2. J Therm Anal Calorim. 2013;111:475–82.
25. Price D, Horrocks AR, Akalin M, Faroq AA. Influence of flame retardants on the mechanism of pyrolysis of cotton (cellulose) fabrics in air. J Anal Appl Pyrolysis. 1997;40–41:511–24.
26. Poon CK, Kan CW. Effects of TiO_2 and curing temperatures on flame retardant finishing of cotton. Carbohyd Polym. 2015;121:457–67.
27. Zhang KK, Zhong L, Tan YQ, et al. Improve the flame retardancy of cellulose fibers by grafting zinc ion. Carbohyd Polym. 2016;136:121–7.
28. Dahiya JB, Kumar K. Flame retardant study of cotton coated with intumescents: kinetics and effect of metal ions. J Sci Ind Res India. 2009;68:548–54.
29. Gann S, Sun G. Effect of phosphorus flame retardants on thermo-oxidative decomposition of cotton. Polym Degrad Stabil. 2007;92:968–74.
30. Kaur R, Gera P, Jha MK, Bhaskar T. Pyrolysis kinetics and thermodynamic parameters of castor (Ricinus communis) residue using thermogravimetric analysis. Bioresour Technol. 2018;250:422–8.
31. Farjas J, Roura R. Isoconversional analysis of solid state transformations—a critical review. Part I. Single step transformations with constant activation energy. J Therm Anal Calorim. 2011;105:757–66.
32. Vyazovkin S, Burnham AK, Criado JM, Pérez-Maqueda LA, Popescu C, Sbirrazzuoli N. ICTAC Kinetics Committee recommendations for performing kinetic computations on thermal analysis data. Thermochim Acta. 2011;520:1–19.
33. Kissinger HE. Variation of peak temperature with heating rate in differential thermal analysis. J Res Natl Bur Stand. 1956;57:217–21.

34. Akahira T, Sunose T. Method of determining activation deterioration constant of electrical insulating materials. Res Rep Chiba Inst Technol (Sci Technol). 1971;16:22–31.

35. Ozawa T. A new method of analyzing thermogravimetric data. Bull Chem Soc Jpn. 1965;38:1881–6.

36. Flynn JH, Wall LA. A quick, direct method for the determination of activation energy from thermogravimetric data. J Polym Sci Part B Poly Lett. 1968;6(4):323–8.

37. Starink MJ. The determination of activation energy from linear heating rate experiments: a comparison of the accuracy of isoconversional methods. Thermochim Acta. 2003;404:163–76.

38. Chen JB, Wang YH, Lang XM, et al. Evaluation of agriculture residues pyrolysis under non-isothermal conditions: thermal behaviors, kinetics, and thermodynamics. Bioresour Technol. 2017;241:340–8.

39. Qu LJ, Wang ZY, Qian J, et al. Effect of combined aluminum-silicon synergistic impregnation and heat treatment on the thermal stability, chemical components, and morphology of wood. BioResources. 2019;14(1):349–62.

40. Nassar MM, Fadali OA, Khattab MA. Thermal studies on paper treated with flame-retardant. Fire Mater. 1999;23:125–9.

41. Ven TVD, Godbout L. Cellulose: fundamental aspects. London: IntechOpen; 2013.

42. Soares S, Richardo NMPS, Jones S, Heatley F. High temperature thermal degradation of cellulose in air studied using FTIR and 1H and 13C solid-state NMR. Eur Polym J. 2001;37:737–45.

43. Tejada C, Herrera A, Ruiz E. Kinetic and isotherms of biosorption of Hg(II) using citric acid treated residual materials. Ing. Compet. 2016;18(1):117–27.

44. Brancatelli G, Colleoni C, Massafra MR, Rosace G. Effect of hybrid phosphorus-doped silica thin films produced by sol-gel

method on the behavior of cotton fabrics. Polym Degrad Stabil. 2011;96:483–90.

45. Horrocks AR. Developments in flame retardants for heat and fire resistant textiles-the role of char formation and intumescence. Polym Degrad Stabil. 1996;54(2–3):143–54.

46. Zhang MR, Rang GQ, Yao YB, et al. Study on structure and properties of silicon-Nitride flame retardant viscose fiber. Synth Fiber China. 2019;48(6):18–23.

47. Deka M, Saikia CN, Baruah KK. Studies on thermal degradation and termite resistant properties of chemically modified wood. Bioresour Technol. 2002;84:151–7.

48. Yorulmaz SY, Atimtay AT. Investigation of combustion kinetics of treated and untreated waste wood samples with thermogravimetric analysis. Fuel Process Technol. 2009;90:939–46.

49. Gao M, Pan DX. Study on the thermal degradation of wood treated with amino resin and amino resin modified with phosphoric acid. J Fire Sci. 2003;21:189–201.

50. Zhu FL, Xin Q, Feng QQ, et al. Influence of nano-silica on flame resistance behavior of intumescent flame retardant cellulosic textiles: remarkable synergistic effect? Surf Coat Technol. 2016;294:90–4.

51. Yao F, Wu QL, Lei Y, Guo WH, Xu YJ. Thermal decomposition kinetics of natural fibers: activation energy with dynamic thermogravimetric analysis. Polym Degrad Stabil. 2008;93(1):90–8.